Full Sky Astrometric Mapping Explorer, FAME, CCD Centroiding Experiment

Kenneth Triebes, Larry Gilliam, Timothy Hilby, Scott Horner, Patrick Perkins, Richard Vassar
Lockheed Martin Advanced Technology Center
3251 Hanover St.
Palo Alto, CA 94304

Fred Harris, David Monet
U.S. Naval Observatory
Flagstaff, AZ

ABSTRACT

FAME is a MIDEX astrometry mission designed to map the positions of 40,000,000 stars to an accuracy of 50 micro-arc seconds. Optimized between mission requirements, size, weight, and cost, the FAME instrument consists of a 0.6 x 0.5 m^2 aperture whose point spread function central peak is linearly sampled by two pixels. To achieve its astrometric mapping mission requirements, this instrument must achieve a single look centroiding accuracy on a visual magnitude 9.0 (or brighter) star of <0.003 pixels while operating the focal plane in a time domain integration, TDI, mode. As this performance requirement represents a significant improvement over the current state of the art of 0.02 to 0.01 pixel resolution, a risk reduction experiment was conducted to determine our centroiding ability using a flight traceable CCD operated in TDI mode. An ultra-stable optical system was configured to project a simulated starfield onto the CCD which was mounted on a high precision moveable stage. Moving the stage across the projected starfield in synchronization with the TDI rate simulated the sensing environment expected in the final instrument, and intensities were adjusted to simulate 9th visual magnitude stars. Experimental results demonstrated single look centroiding accuracy of <0.002 pixels in addition to yielding unexpected dividends in refining CCD operations and centroid data analysis. This paper describes the experiment design, centroiding results, CCD operating techniques and data analysis methods.

Introduction

The objective of the FAME mission will be to measure the positions, proper motions, parallaxes, and four-color magnitudes of 40 million stars brighter than 15th visual magnitude during the observational program. Positional accuracy will be the best yet achieved with stellar position, parallax, and proper motion accuracy's better than 50 μas, 50 μas, and 50 μas/year, respectively. The spacecraft will be placed in a geosynchronous orbit, with a rotational axis 45^o from the Sun, rotating with a 20-minute period which precesses around the Sun direction every 10 days. FAME will sweep the sky repeatedly, in a pattern similar to the Hipparcos project. The mission life is 2.5 years, with a potential extended mission life of 5 years.

The instrument architecture, Figure 1, is the result of a two-year design study combined with the heritage of the successful ESA mission, Hipparcos (Perryman et al. 1989). The main results of the study are documented in a pair of SPIE papers (Reasenberg & Phillips 1998; Phillips & Reasenberg 1998). FAME takes from Hipparcos its two essential geometric characteristics, (1) two widely separated FOVs that are combined on a single detection plane, and (2) a scan pattern that involves both a nominal spin axis orthogonal to the look directions and precession of that spin axis around the Sun direction. The science instrument optical train begins with a compound mirror looking in two directions separated by an angle of 81.5^o. The two fields of view are simultaneously imaged through a common telescope and combined on a focal plane having 20 astrometric charge coupled detector (CCD) arrays and four photometric CCDs. Based on a three-mirror anastigmat folded optical design, the telescope provides a flat, diffraction limited field of view over the full detector array. CCD's are operated in a time delay integration (TDI) mode with the readout rate maintained at the spacecraft spin rate providing integration time for the observations. The pixels with stellar images are read out, time tagged, and transmitted to the ground station. Resolution across the unresolved stellar images is 2.4 pixels per central lobe of the optical system point spread function.

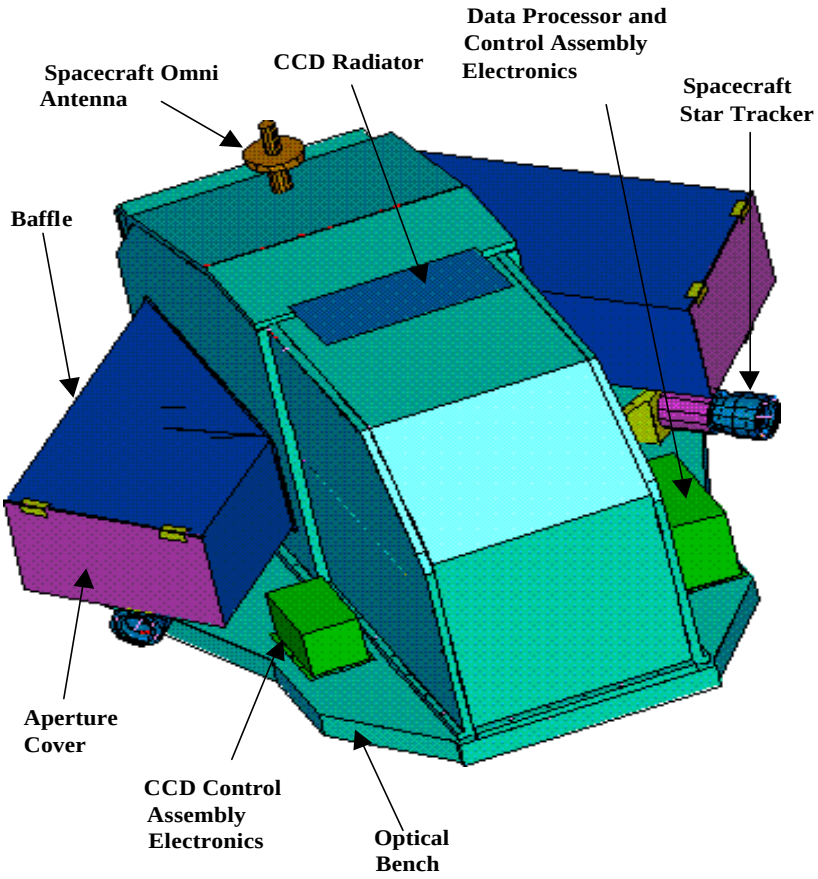

Figure 1. Schematic view of FAME instrument.

As a result of optimizing the payload design between mission requirements and the constraints of size, weight, and cost, the single-look centroiding accuracy requirement for a visual magnitude 9.0 star was established at <0.003 pixels while operating the focal plane in a TDI mode. This performance requirement represents a significant improvement over the current state of the art of 0.02 to 0.01 pixels resolution and was listed as an issue of concern for the system design. To demonstrate the achievability of this precision, a risk reduction experiment was designed and conducted using a simulated starfield and a flight traceable CCD operated in a TDI mode.

Objective

The objective of the FAME centroiding experiment was to demonstrate that the required single look centroiding precision could be achieved in a simulated operating environment using a traceable CCD detector array. A simulated multi-spectral starfield was swept across the focal plane in synchronization with the TDI readout rate. Issues to be simulated in the experiment design were the stellar spectrum, the star images scaled to the CCD pixel sizes and matched to the point spread function shape as defined by the FAME optical prescription, and the star brightness. Critical factors in the experiment design were opto-mechanical stability, and the ability to precisely coordinate the CCD TDI rate with the starfield scanning system.

Approach

The schematic design of the centroiding experiment is shown in Figure 2. It consists of a starfield projector which produces scaled multi-spectral point spread functions and a flight-traceable CCD focal plane mounted on a precision linear stage to simulate the linear sweep of the starfield across the detector array. Star images are produced with an array of 16 single-mode optical fibers bonded into an aluminum block to ensure the stability of their relative positions. The fibers are illuminated with a white light source having a color temperature around 3100 K. A lens

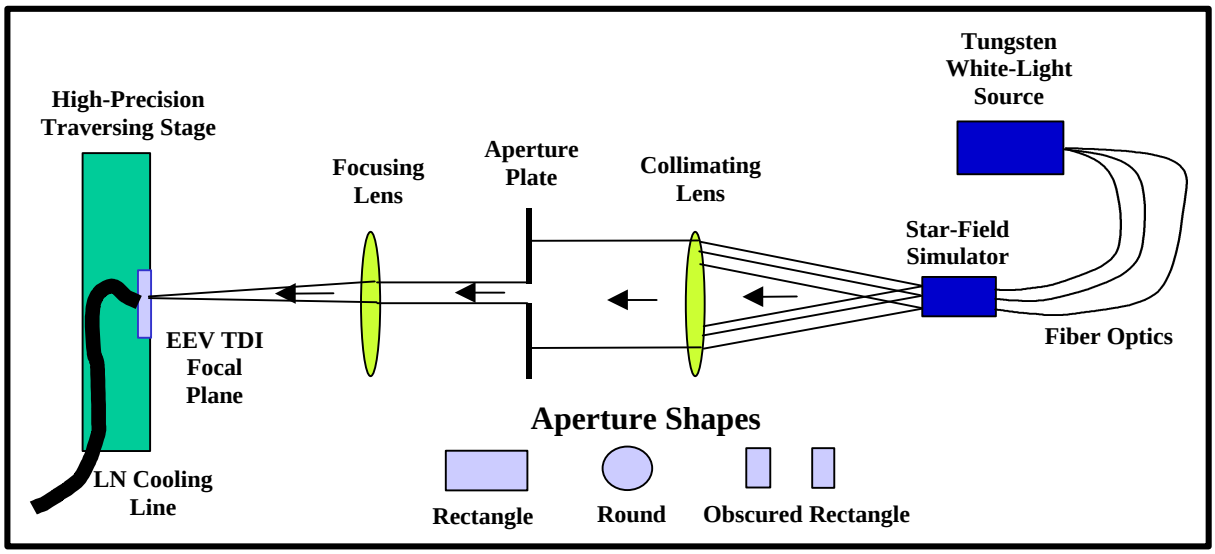

Figure 2. FAME Centroiding Experiment Layout.

collimates the stellar images, which are then focused onto the CCD array by a second lens. Between the lenses is an aperture mask whose options include the various pupil geometry's under consideration for the FAME instrument. Aperture geometry options included circular, rectangular, and a rectangle with a central obscuration. Original experiment plans called for generating comparative data with all three aperture geometry's, however, schedule permitted the use of only the rectangular and circular options. The linear stage used to sweep the CCD across the starfield images was a commercially available device manufactured by Aerotech Inc. of Pittsburgh, PA, Model ALS20030. Its total range of motion was 100 mm with sweep velocities ranging from 0.1 to 100 mm/sec. The CCD array was supplied by the U.S. Naval Observatory at Flagstaff, AZ. It was manufactured by EEV, model CCD 42-80, and had a geometry of 2048x4096 pixels.

Experiment Operation

Figure 3 shows a photograph of the experiment set-up. All components are mounted on a vibration isolated optical bench and the experiment was conducted in vacuum. This eliminated the random influence of the atmosphere on the optical path and also prevented condensation on the CCD, which was operated at a temperature of 170 K to reduce dark current effects. The CCD was thermally isolated from the translation stage to eliminate the possibility of temperature gradients adversely effecting stage operation. Critical components were equipped with remote actuation to allow refinement of the alignment during vacuum operation. The aperture mask was actuated to allow dithering which provided a positive test of focus precision prior to taking centroiding data.

Following pump-down, the CCD array was initially operated in a staring mode both to ensure its operability and to refine the focus of the projected star field. Lateral translation of the aperture plane in a dither mode was used to refine the focus, which was adjusted by moving the fiber optic point source array. For taking centroid data, the CCD array could be operated in a variety TDI of modes. The first mode was a standard "bucket-brigade" where the charge is transferred in single pixel increments in sync with the motion of the image. This mode was used with the rectangular unobscured aperture. Image smear was minimized through careful synchronization of the linear stage motion with the TDI rate. In the standard TDI mode the minimum smear observed was approximately 1.0 pixels and was attributed to the difference between smooth image motion and the stair-step charge transfer. The standard TDI clocking mode consistently resulted in the narrowest stellar images and produced the best centroiding data.

The second TDI mode to be investigated was a "constant-phase" clocking where the charge was moved in 1/6 pixel increments which were equally spaced in time. The sub-pixel charge transfer resulted in photon collection in individual pixels that alternated between 1/3 and 2/3 of a pixel. It was felt that this mode may have resulted in enhanced image smear. This mode was used with the circular aperture for projecting the simulated star field.

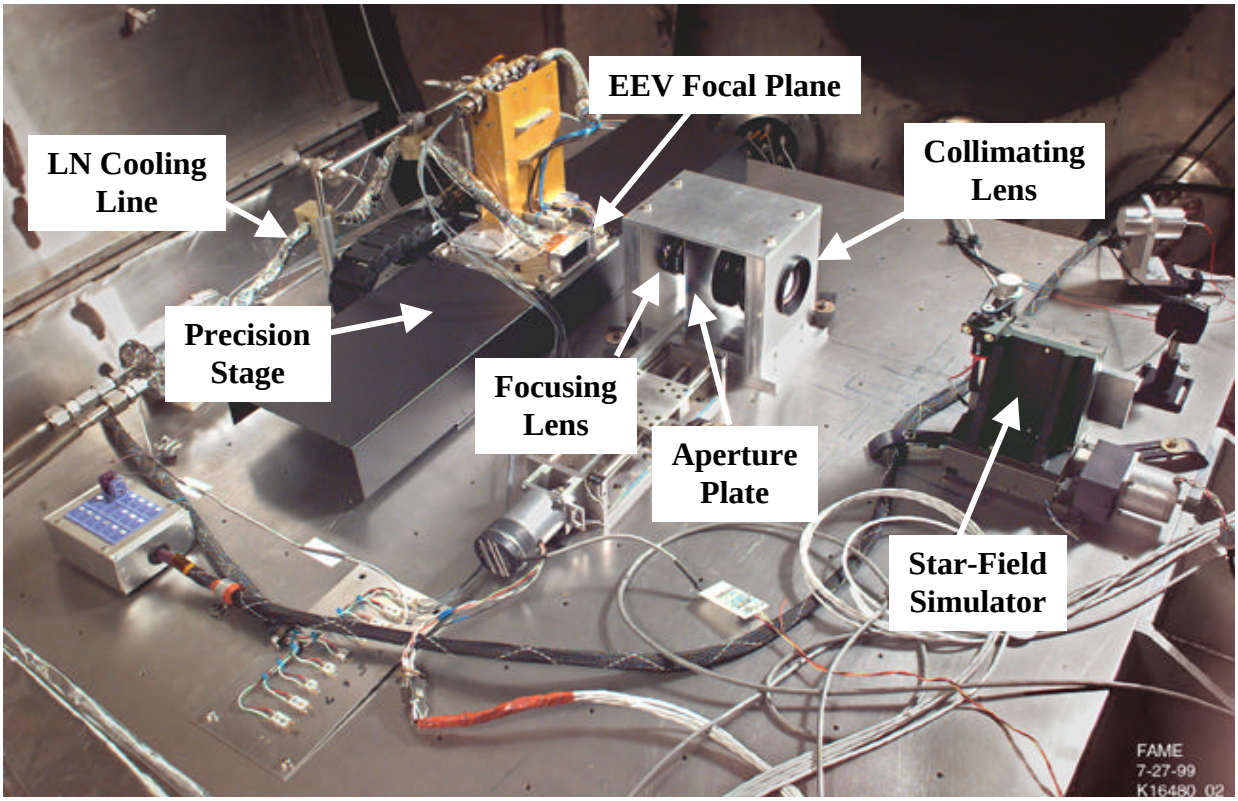

Figure 3. Photo of centroiding experiment set-up.

Although there was insufficient time for a complete characterization, the image sizes were larger and the centroiding precision less for this CCD operating mode presumably due to the enhanced image smear.

Data Analysis

The files generated by the simulation experiment were first translated into the astronomical standard FITS format, and then each was examined visually. During the visual examination, the operator set a cursor on each image deemed measurable (not too close to the edge of the CCD, sensibly away from bad columns, etc.). These settings, which are accurate to approximately +/-1 pixel, were used as the initial guess for all centroiding algorithms examined in this study.

Three centroiding algorithms were examined. The first, called 1D, fits separate Gaussians to the X and Y marginal distributions of the image. In a landmark paper in the 1970s, Auer and van Altena demonstrated that this algorithm was a robust estimator for the position of astronomical image and was substantially cheaper than fitting the 2-dimensional array of pixel data. Over two decades of digital astrometry have proven the correctness of the basic conclusion, namely that this was a good and cheap algorithm, but if enough CPU cycles are available, 2-dimensional algorithms can produce somewhat higher accuracy. Under normal circumstances, this algorithm can deliver accuracy's on the order of 0.01 pixel, and provides a decent measure of the position of objects with peculiar point spread functions. Hence, it is used as a basic sanity test for all other algorithms.

The second algorithm examined was a fit to a 2-dimensional representation of the FAME PSF. Normalized template PSFs were generated on a grid of 0.001x0.001 pixels, and were computed from the weighted sum of 13 monochromatic FAME PSF's computed according to the optical prescription. The relative weights were appropriate for a 3100K blackbody. The choice of pre-computing this PSF on a sub-pixel lattice flows from the numerical complexity of the function, the difficulty in taking analytic derivatives, and the expectation of the enormous size of the FAME database. For reasons that are not obvious, this algorithm is referred to as the 4D code.

The third algorithm examined is a popular favorite, namely fitting the image profile to a Gaussian with an elliptical cross-section. This was chosen because visual examination of the images showed that the combined effects of scan rate mismatch, the polychromatic nature of the illumination, and other blurring effects makes the images look

something like lumps, and makes the diffraction rings almost invisible. A traditional astrometric approach to fitting lumps is to pretend that they are Gaussian, and to hope that differences between the Gaussian and the true PSF will appear as systematic trends rather than increased dispersion as a function of the sub-pixel placement of the image. This is referred to as the 5D code.

Given a list of centers, in this case computed from either the 1D, 4D, or 5D codes, the determination of the astrometric properties of the CCD follows a traditional numerical relaxation calculation. If one knew the mean positions of the images, then one could compute the coefficients that map a particular frame to the mean coordinates. If one knew the mapping of the frames, one could compute the mean position of each image. Since one knows neither the mean positions nor the mapping coefficients, one takes the positions of the images on a single frame, pretends that they are the mean positions, and solves for the mapping coefficients. This process is iterated until neither the mean positions nor the mapping coefficients change between iterations. Convergence is rapid and unique for normal, non-pathological instances such as the data generated from the FAME stimulus. The deviation of the individual measures from the means are usually less than 0.01 pixel, and the mapping coefficients, presumed linear in this test, are surprisingly close to unity with the exception of the offset between frames.

The reduction of the 1D, 4D, and 5D centers was routine, and several sanity tests were passed. First, the 1D results were reasonable and the 4D and 5D results were somewhat better. Second, and more importantly, no measures had to be rejected from any solution. This point can be quite important. There is always the possibility that a cosmic ray, a problem in applying the flat field correction, or some other process can contaminate the pixel values in an image. Visual examination is quite inadequate for verifying that image contamination is not present, and the only real way to sense these problems is to find statistically unreasonable residuals. One should be seriously worried if a significant number of measurements must be omitted on the basis of large residuals. This might be the result of a failure of the centroiding process at particular locations in a pixel, and that omitting these measures will systematically bias the deduced position for the star. Again, for these tests all measures of all stars using all centering algorithms had reasonable residuals, and none had to be omitted.

The following variables were used in developing the analysis model used in evaluating the FAME centroiding data.

Variables

n	– number of point-sources (stars) in image frame
m	– number of image frames per test
A	– unbiased image frame matrix
R	– range of rows indices which center the desired mode
C	– range of column indices which center the desired mode
xc	– uncompensated x-axis centroid coordinate
yc	– uncompensated y-axis centroid coordinate
mx	– distance from x-axis mode to uncompensated x-axis centroid
my	– distance from y-axis mode to uncompensated y-axis centroid
xa	– compensated x-axis centroid coordinate estimate
ya	– compensated y-axis centroid coordinate estimate
$XC^{<j>}$	– vector of uncompensated x-axis centroid coordinates of each star in the *j*th image frame
$YC^{<j>}$	– vector of uncompensated y-axis centroid coordinates of each star in the *j*th image frame
$mXc^{<j>}$	– vector of distances from x-axis mode to the uncompensated x-axis centroid for each star in the *j*th image frame
$mYc^{<j>}$	– vector of distances from y-axis mode to the uncompensated y-axis centroid for each star in the *j*th image frame
XA	– vector of compensated x-axis centroid coordinate estimates of stars in initial frame coordinates
YA	– vector of compensated y-axis centroid coordinate estimates of stars in initial frame coordinates
kX	– x-axis centroid correction factor
kY	– y-axis centroid correction factor
dXA	– vectors of x-axis displacements of each frame relative to the first frame
dYA	– vectors of y-axis displacements of each frame relative to the first frame
QA	– vector of rotations of each frame relative to the first frame

FAME Centroiding Algorithm

In order to estimate the precise (relative) positions of point sources (stars) in an image frame to sub-pixel accuracy, the following algorithm was proposed.

1. Remove the dark frame bias. Because of manufacturing variability and thermal effects, each pixel may be expected to have a "bias" value associated with the pixel output intensity under the condition of zero input intensity. These biases may be measured by periodically imaging a dark frame. Thereafter, each image frame may be corrected by subtracting the dark frame:
2. Identify the general region in the image frame of the point source of interest.
3. Find the row mode (mode of the sum of columns) and column mode (mode of the sum of rows) within the region.
4. Choose a range of rows, R, which centers the row mode, and columns, C, which centers the column mode. Select an odd number of pixel elements for R and C so that the row mode is located at the row coordinate given by $median(R)$ and the column mode is located at the column coordinate given by $median(C)$. The number of pixel elements should be chosen such that most of the energy of the point spread function is included within the range of R and C.
5. Compute the image centroid (first moments) over the range described by R and C.

$$\begin{bmatrix} xc \\ yc \end{bmatrix} = \frac{1}{\sum_{i \in C} \sum_{j \in R} A_{i,j}} \cdot \begin{bmatrix} \sum_{i \in C} \sum_{j \in R} A_{i,j} \cdot i \\ \sum_{i \in C} \sum_{j \in R} A_{i,j} \cdot j \end{bmatrix} \qquad [1]$$

The resulting centroid estimate is known to contain an error dependent upon the pixel size, point spread function of the aperture, and the number of pixels used to estimate the centroid. This error arises due to the truncation of the tails of the point-spread function by the centroiding algorithm. Modeling of this error has led to the following correction.

6. Correct the centroid estimate.
   The centroid estimate is corrected in each axis by an amount proportional to the distance along that axis from the axis mode to the centroid estimate (This quantity should range from –1/2 to +1/2 pixel).

$$\begin{bmatrix} mx \\ my \end{bmatrix} = \begin{bmatrix} xc - median(C) \\ yc - median(R) \end{bmatrix} \qquad [2]$$

$$\begin{bmatrix} xa \\ ya \end{bmatrix} = \begin{bmatrix} xc \\ yc \end{bmatrix} + \begin{bmatrix} kX & 0 \\ 0 & kY \end{bmatrix} \cdot \begin{bmatrix} mx \\ my \end{bmatrix} \qquad [3]$$

The correction factors, kX and kY, are constant for a given pixel size, point spread function, and number of pixels used to compute the centroid. Although, these values may be estimated from an a priori model, they may also be calibrated by experiment.

Data Processing

Starting with a star field with *n* stars, *m* image frames of the *n* stars are recorded. Because of variability in timing the start of TDI, the images may be displaced from one another in the rows-axis. Thermal and temporal drift may also cause the images to be displaced from one-another in the columns-axis or rotated relative to one another orthogonal to the image plane.

The objective is to resolve the positions of the stars and the displacements and rotations of the image frames with respect to a common coordinate frame. The choice of a common coordinate frame is somewhat arbitrary, but for the purposes of this analysis was selected to be defined by the first image frame.

We wish to estimate the following quantities from our observations:

XA,YA	- positions of each star in initial frame coordinates (2*m*)
kX, kY	- constant correction factors for PSF centroiding error (2)
dXA, dYA	- displacements of each frame (relative to first frame) (2*m*-2)
QA	- rotation of each frame relative to the first frame (*m*-1)

This gives a total of (2*n* + 3*m* - 1) model degrees of freedom with which we can define a model state vector:

$$\vec{x} = \begin{bmatrix} XA \\ YA \\ kX \\ kY \\ dXA \\ dYA \\ QA \end{bmatrix} \qquad [4]$$

If steps 1 through 5 of the centroiding algorithm described above are carried out for all stars of interest in each image frame, there will be a single measurement pair (uncompensated centroid) for each star in each frame. This gives a total of (2*nm*) measurement degrees of freedom.

$XC^{<j>}$	- vector of uncompensated x-axis centroids for stars in *j*th image frame (*n*)
$YC^{<j>}$	- vector of uncompensated y-axis centroids for stars in *j*th image frame (*n*)

In addition, there will be a pair of distances from the modal axes to the centroid for each star in each frame. However, since these values are calculated from the uncompensated centroids, they do not contribute to the measurement degrees of freedom.

$mXc^{<j>}$	- distances from the modal y-axes to the uncompensated x-axis centroids for the stars in *j*th image frame (*n*)
$mYc^{<j>}$	- distances from the modal x-axes to the uncompensated y-axis centroids for the stars in *j*th image frame (*n*)

Since the measurement degrees of freedom minus the model degrees of freedom yields the residual degrees of freedom: There will be [(2*nm*) – (2*n* + 3*m* –1)] residual degrees of freedom.

Thus, the problem can be written in terms of (2*nm*) equations in (2*n* + 3*m* - 1) unknowns:

$$\vec{v} = \begin{bmatrix} \begin{bmatrix} XA \\ YA \end{bmatrix} \\ \begin{bmatrix} XA \\ YA \end{bmatrix} \\ \begin{bmatrix} XA \\ YA \end{bmatrix} \\ \vdots \\ \begin{bmatrix} XA \\ YA \end{bmatrix} \end{bmatrix} - \begin{bmatrix} \begin{bmatrix} 0_{n\times 1} \\ 0_{n\times 1} \end{bmatrix} \\ \begin{bmatrix} dXA(1)_{n\times 1} \\ dYA(1)_{n\times 1} \end{bmatrix} \\ \begin{bmatrix} dXA(2)_{n\times 1} \\ dYA(2)_{n\times 1} \end{bmatrix} \\ \vdots \\ \begin{bmatrix} dXA(m-1)_{n\times 1} \\ dYA(m-1)_{n\times 1} \end{bmatrix} \end{bmatrix} - \begin{bmatrix} \begin{bmatrix} XC^{\langle 1\rangle} + kX \cdot mXc^{\langle 1\rangle} \\ YC^{\langle 1\rangle} + kY \cdot mYc^{\langle 1\rangle} \end{bmatrix} \\ \begin{bmatrix} \cos(QA(1))\cdot I_{n\times n} & -\sin(QA(1))\cdot I_{n\times n} \\ \sin(QA(1))\cdot I_{n\times n} & \cos(QA(1))\cdot I_{n\times n} \end{bmatrix} \cdot \begin{bmatrix} XC^{\langle 2\rangle} + kX \cdot mXc^{\langle 2\rangle} \\ YC^{\langle 2\rangle} + kY \cdot mYc^{\langle 2\rangle} \end{bmatrix} \\ \begin{bmatrix} \cos(QA(2))\cdot I_{n\times n} & -\sin(QA(2))\cdot I_{n\times n} \\ \sin(QA(2))\cdot I_{n\times n} & \cos(QA(2))\cdot I_{n\times n} \end{bmatrix} \cdot \begin{bmatrix} XC^{\langle 3\rangle} + kX \cdot mXc^{\langle 3\rangle} \\ YC^{\langle 3\rangle} + kY \cdot mYc^{\langle 3\rangle} \end{bmatrix} \\ \vdots \\ \begin{bmatrix} \cos(QA(m-1))\cdot I_{n\times n} & -\sin(QA(m-1))\cdot I_{n\times n} \\ \sin(QA(m-1))\cdot I_{n\times n} & \cos(QA(m-1))\cdot I_{n\times n} \end{bmatrix} \cdot \begin{bmatrix} XC^{\langle m\rangle} + kX \cdot mXc^{\langle m\rangle} \\ YC^{\langle m\rangle} + kY \cdot mYc^{\langle m\rangle} \end{bmatrix} \end{bmatrix}$$

[5]

The error vector gradient may be written as…

$$\frac{\partial \vec{v}}{\partial \vec{x}} = \begin{bmatrix} I_{n\times n} & 0_{n\times n} & -mXc^{\langle 1\rangle} & 0_{n\times 1} & 0_{n\times(m-1)} & 0_{n\times(m-1)} & 0_{n\times(m-1)} \\ 0_{n\times n} & I_{n\times n} & 0_{n\times 1} & -mYc^{\langle 1\rangle} & 0_{n\times(m-1)} & 0_{n\times(m-1)} & 0_{n\times(m-1)} \\ I_{n\times n} & 0_{n\times n} & -\cos(QA(1))\cdot mXc^{\langle 2\rangle} & \sin(QA(1))\cdot mYc^{\langle 2\rangle} & -\begin{bmatrix}1_{n\times 1} & 0_{n\times 1} & \cdots & 0_{n\times 1}\end{bmatrix} & 0_{n\times(m-1)} & \begin{bmatrix}YB^{\langle 2\rangle} & 0_{n\times 1} & \cdots & 0_{n\times 1}\end{bmatrix} \\ 0_{n\times n} & I_{n\times n} & -\sin(QA(1))\cdot mXc^{\langle 2\rangle} & -\cos(QA(1))\cdot mYc^{\langle 2\rangle} & 0_{n\times(m-1)} & -\begin{bmatrix}1_{n\times 1} & 0_{n\times 1} & \cdots & 0_{n\times 1}\end{bmatrix} & -\begin{bmatrix}XB^{\langle 2\rangle} & 0_{n\times 1} & \cdots & 0_{n\times 1}\end{bmatrix} \\ I_{n\times n} & 0_{n\times n} & -\cos(QA(2))\cdot mXc^{\langle 3\rangle} & \sin(QA(2))\cdot mYc^{\langle 2\rangle} & -\begin{bmatrix}0_{n\times 1} & 1_{n\times 1} & \cdots & 0_{n\times 1}\end{bmatrix} & 0_{n\times(m-1)} & \begin{bmatrix}0_{n\times 1} & YB^{\langle 3\rangle} & \cdots & 0_{n\times 1}\end{bmatrix} \\ 0_{n\times n} & I_{n\times n} & -\sin(QA(2))\cdot mYc^{\langle 3\rangle} & -\cos(QA(2))\cdot mYc^{\langle 3\rangle} & 0_{n\times(m-1)} & -\begin{bmatrix}0_{n\times 1} & 1_{n\times 1} & \cdots & 0_{n\times 1}\end{bmatrix} & -\begin{bmatrix}0_{n\times 1} & XB^{\langle 3\rangle} & \cdots & 0_{n\times 1}\end{bmatrix} \\ \vdots & \vdots & \vdots & \vdots & \vdots & \vdots & \vdots \\ I_{n\times n} & 0_{n\times n} & -\cos(QA(m-1))\cdot mXc^{\langle m\rangle} & \sin(QA(m-1))\cdot mYc^{\langle m\rangle} & -\begin{bmatrix}0_{n\times 1} & 0_{n\times 1} & \cdots & 1_{n\times 1}\end{bmatrix} & 0_{n\times(m-1)} & \begin{bmatrix}0_{n\times 1} & 0_{n\times 1} & \cdots & YB^{\langle m\rangle}\end{bmatrix} \\ 0_{n\times n} & I_{n\times n} & -\sin(QA(m-1))\cdot mYc^{\langle m\rangle} & -\cos(QA(m-1))\cdot mYc^{\langle m\rangle} & 0_{n\times(m-1)} & -\begin{bmatrix}0_{n\times 1} & 0_{n\times 1} & \cdots & 1_{n\times 1}\end{bmatrix} & -\begin{bmatrix}0_{n\times 1} & 0_{n\times 1} & \cdots & XB^{\langle m\rangle}\end{bmatrix} \end{bmatrix}$$

[6]

Where,

$$\begin{bmatrix} XB^{\langle i\rangle} \\ YB^{\langle i\rangle} \end{bmatrix} = \begin{bmatrix} \cos(QA(i-1)) & -\sin(QA(i-1)) \\ \sin(QA(i-1)) & \cos(QA(i-1)) \end{bmatrix} \cdot \begin{bmatrix} XC^{\langle i\rangle} + kX\cdot mXc^{\langle i\rangle} \\ YC^{\langle i\rangle} + kY\cdot mYc^{\langle i\rangle} \end{bmatrix} \quad ; \quad i \in \{1\ldots m\} \qquad [7]$$

To solve for the state vector, an initial estimate is provided. The uncorrected centroid measurements from the first image frame provide an excellent initialization point for the corrected centroid estimates. Other states are initialized to zero (no a priori knowledge assumed).

$$\vec{x} = \begin{bmatrix} XC^{\langle 1\rangle} \\ YC^{\langle 1\rangle} \\ 0 \\ 0 \\ 0_{(m-1)\times 1} \\ 0_{(m-1)\times 1} \\ 0_{(m-1)\times 1} \end{bmatrix} \qquad [8]$$

Then, iterate the following equations until the state estimate converges.

1. Compute the error vector, $\vec{v}$, as a function of the current state estimates as described by equation 5.
2. Compute the error vector gradient, $\left(\frac{\partial \vec{v}}{\partial \vec{x}}\right)$, as a function of the current state estimates described by equation 6.
3. Update the state estimate. $$\vec{x} = \vec{x} - \left(\left(\frac{\partial \vec{v}}{\partial \vec{x}}\right)^T \left(\frac{\partial \vec{v}}{\partial \vec{x}}\right)\right)^{-1} \left(\frac{\partial \vec{v}}{\partial \vec{x}}\right)^T \cdot \vec{v} \qquad [9]$$

Results

One of the tests conducted used a field consisting of ten point-sources (n=10), which was imaged twenty-five times (m=25). Positions of the point sources in pixel units as seen in the first image are shown in Figure 4.

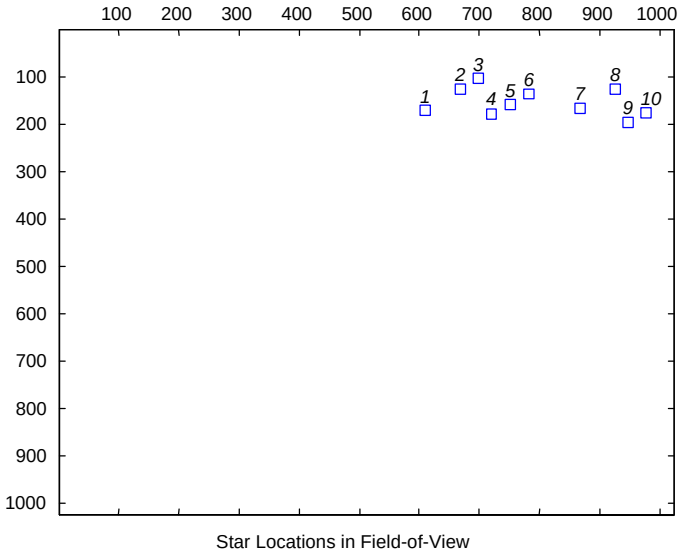

Figure 4 Star locations in the CCD field of view in pixel units.

Residual errors are summarized in figures 5 and 6. Figure 5 shows a scatter plot of the y-axis estimation error vs. the x-axis estimation errors for all stars and all image frames. Figure 6 shows a histogram of the y-axis errors.

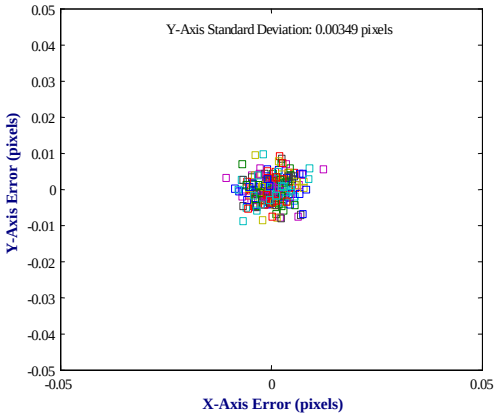

Figure 5. Scatterplot of the X and Y axis centroiding errors for the full simulated star field.

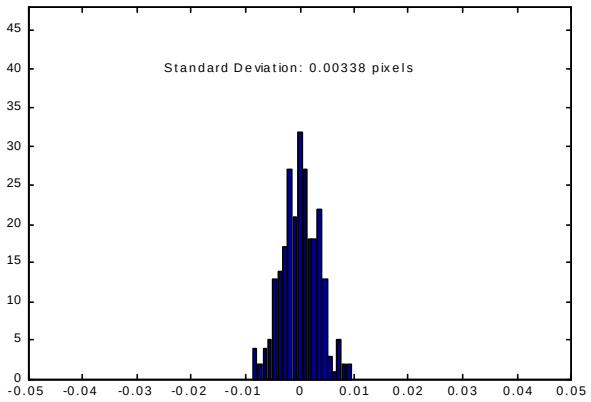

Figure 6. Histogram of Y-axis estimation errors for the full star field.

Several of the point sources in this particular example were relatively dim. Further tests demonstrated improvements in centroiding accuracy when only bright point sources were used.

As a result of the fabrication techniques used to make the star field simulator, the brightness of the individual images varied by a factor of two. To obtain better correlation for the final statistical analysis, the four brightest stars in the field were selected for further analysis. Their relative brightness varied less than $\pm$3% with respect to one another. Two data sets were taken, one with the rectangular aperture where the standard TDI CCD clocking mode was used. The second data set used the circular aperture and the CCD was clocked in the constant phase TDI mode. Figure 7 shows the results of the first data set, rectangular aperture and standard TDI CCD clocking, which includes 25 scans of the star field across the CCD and is a plot of the X and Y axis errors for the individual stars. For this data set, the Y-axis standard deviation was 0.00198 pixels against the requirement of 0.0029 pixels. In order to test for systematic errors in the data analysis techniques, the Y-axis errors were plotted against the distance from the

centroid to the mode, Figure 8. The flat band of error data indicates no observable systematic error in the final data. Figures 9 and 10 show the same format data plots for the circular aperture with the constant-phase CCD clocking mode. In this case, a total of 39 data scans are presented and the final Y-axis error is 0.00254 pixels against the requirement of 0.0029.

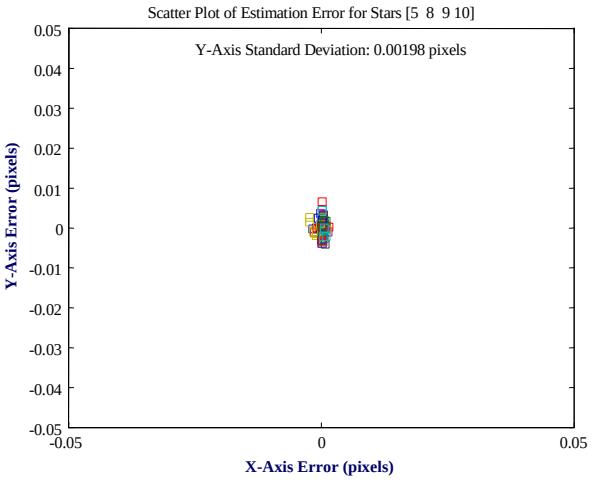

Figure 7. Centroid estimation errors for brightest stars using standard TDI CCD clocking.

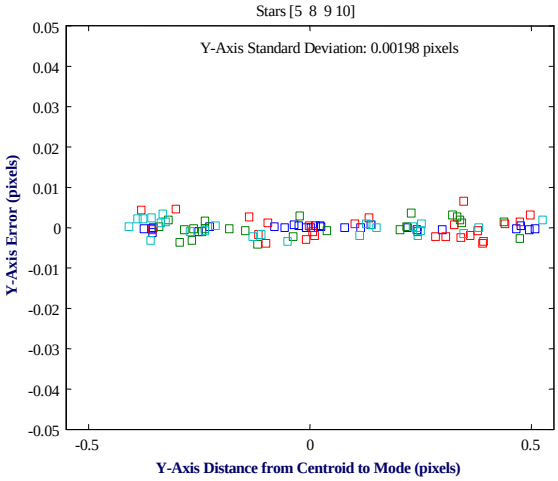

Figure 8. Centroid errors Vs distance from mode for standard TDI CCD clocking.

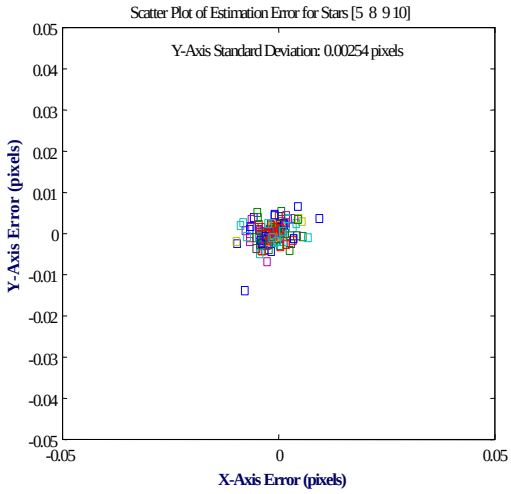

Figure 9. Centroid estimation errors for brightest stars using constant-phase TDI CCD clocking.

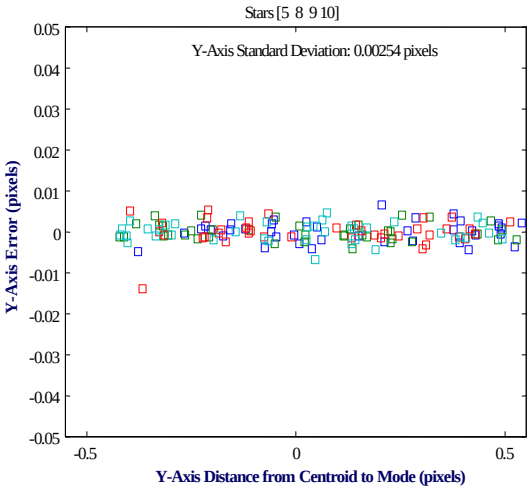

Figure 10. Centroid errors Vs distance from mode for constant-phase TDI CCD clocking.

Conclusions

Experimental results have demonstrated that there is no fundamental limitation to achieving the centroiding accuracy specified for the FAME payload. Two methods for clocking the CCD array in the TDI mode were examined and characterized in a preliminary manner. Both clocking methods met the single look accuracy requirement, however, the standard clocking produced better results presumably as a result of less image smear. Due to time constraints on the experiment, it was not possible to determine reasons for the performance differences between the two clocking modes. Matching the image motion to the TDI rate was found to be critical for maximum accuracy, again, to minimize image smear. Follow-on investigations will include a more thorough characterization of CCD clocking options in addition to evaluating the bi-phase method, which could not be included in the first

experiments. It will also include an investigation of the effects of star color temperature on centroiding accuracy and data reduction algorithms.

Acknowledgements

This work was jointly sponsored by the Lockheed Martin Advanced Technology Center and the U.S. Naval Observatory.

References

Auer, L.H., and van Altena, W. F. (1978) Astronomical Journal vol. 83, page 531
Perryman, M. A. C. et al., 1989, “The Hipparcos Mission”, ESA SP-1111 vol. 3
Phillips, J.D. and Reasenberg, R.D., 1998, “Optical System for an Astrometric Survey from Space,” SPIE 3356
Reasenberg, R.D., and Phillips, J.D., 1998, “Design of a Spaceborne Astrometric Survey Instrument,” SPIE 3356